

## Electrochemistry and Speciation of Au<sup>+</sup> in a Deep Eutectic Solvent: Growth and Morphology of Galvanic Immersion coatings

Andrew D. Ballantyne,<sup>a</sup> Gregory C. H. Forrest,<sup>a</sup> Gero Frisch,<sup>b</sup> Jennifer M. Hartley<sup>b</sup> and Karl S. Ryder<sup>a†</sup>

Received 00th January 20xx,  
Accepted 00th January 20xx

DOI: 10.1039/x0xx00000x

www.rsc.org/

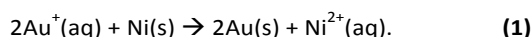
In this study we compare the electrochemical and structural properties of three gold salts AuCl, AuCN and KAu(CN)<sub>2</sub> in a Deep Eutectic Solvent (DES) electrolyte (Ethaline 200) in order to elucidate factors affecting the galvanic deposition of gold coatings on nickel substrates. A chemically reversible diffusion limited response was observed for AuCl, whereas AuCN and KAu(CN)<sub>2</sub> showed much more complicated, kinetically limited responses. Galvanic exchange reactions were performed on nickel substrates from DES solutions of the three gold salts; the AuCN gave a bright gold coating, the KAu(CN)<sub>2</sub> solution give a visibly thin coating, whilst the coating from AuCl was dull, friable and poorly adhesive. This behaviour was rationalised by the differing speciation for each of these compounds, as evidenced by EXAFS methods. Analysis of EXAFS data shows that AuCl forms the chlorido-complex [AuCl<sub>2</sub>]<sup>-</sup>, AuCN forms a mixed [AuCl(CN)]<sup>-</sup> species, whereas KAu(CN)<sub>2</sub> maintains its [Au(CN)<sub>2</sub>]<sup>-</sup> structure. The more labile Cl<sup>-</sup> enables easier reduction of Au when compared to the tightly bound cyanide species, hence leading to slower kinetics of deposition and differing electrochemical behaviour. We conclude that metal speciation in DESs is a function of the initial metal salt and that this has a strong influence on the mechanism and rate of growth, as well as on the morphology of the metal deposit obtained. In addition, these coatings are also extremely promising from a technological perspective as Electroless Nickel Immersion Gold (ENIG) finishes in the printed circuit board (PCB) industry, where the elimination of acid in gold plating formulation could potentially lead to more reliable coatings. Consequently, these results are both significant and timely.

### Introduction

Gold plating processes are widely used in the materials finishing, decorative and electronics industries due to their high reliability, electrical conductivity and corrosion resistance.<sup>1</sup> The key characteristic feature of these noble metal coatings is the lack of insulating surface oxides.<sup>2</sup> Electrolytic,<sup>3</sup> electroless,<sup>4</sup> and immersion plating<sup>5</sup> are the three common electrochemical methods used for the coating of conducting substrates with gold films. In each of these processes the conventional/commercial plating bath chemistry is dominated by the choice of the dicyanidoaurate anion [Au(CN)<sub>2</sub>]<sup>-</sup> as the gold source<sup>6</sup> due to its high stability<sup>7</sup> and the ability to yield fine grained deposits.<sup>8</sup> In electroplating experiments, acidic plating baths around pH 5 are used to produce soft gold coatings, whilst alkaline and neutral baths are used to produce hard gold.<sup>8</sup> However, there are significant safety concerns, as well as issues regarding the disposal of waste, where cyanide

based processes are present. In addition, the requirement of large negative reduction potentials can also lead to the co-reduction of hydrogen ions.<sup>9</sup> As such, there have been cyanide free gold plating solutions developed, primarily based upon sulphite and thiosulfate complexes, however these are limited to electrolytic methodologies.<sup>3</sup>

Galvanic (immersion) coatings are an important electrochemical process for the deposition of the thin gold coatings commonly used in the PCB and electronics industries. These coatings involve the galvanic exchange of a metal substrate with another from solution.<sup>10</sup> One such coating, electroless nickel immersion gold (ENIG), is of particular importance in the maintenance of a solderable surface on printed circuit boards during storage, prior to solder reflow.<sup>11</sup> In this case Ni is liberated from the surface, providing electrons to two gold ions in solution, causing their reduction and creating a thin film of gold on the substrate surface, **Equation 1**.



In the fabrication of ENIG coatings the electroless Ni is deposited on the copper substrate by the catalytic action of a solution phase reducing agent, NaPH<sub>2</sub>O<sub>2</sub>, where the catalyst is a very thin coating of PdCl<sub>2</sub> applied to the copper. As a consequence, the resultant ENIG nickel coating contains 8-12 wt. % phosphorus incorporated from the reducing agent. This

<sup>a</sup> Materials Centre, Department of Chemistry, University of Leicester, University Road, Leicester LE1 7RH, United Kingdom.

<sup>b</sup> Institut für Anorganische Chemie, TU Bergakademie Freiberg, Leipziger Str. 29, 09599 Freiberg, Germany.

† email: ksr7@leicester.ac.uk.

Electronic Supplementary Information (ESI) available: [details of any supplementary information available should be included here]. See DOI: 10.1039/x0xx00000x

is generally favourable for the physical properties of the nickel coating in PCB applications and gives good adhesion and durability as well as providing an essential and effective diffusion barrier for the copper atoms of the substrate.

ENIG is a relatively expensive surface finish for PCBs because of the presence of gold, but despite this, it is increasing in popularity as it produces a surface with good planarity (important for automated electronics assembly) and solderability, even when subjected to multiple heat/cool solder reflow cycles.<sup>12</sup> However, ENIG coatings are susceptible to a phenomenon termed “black pad” which is generally accepted to be oxide formation on the surface of the underlying electroless nickel (EN) substrate, resulting from galvanic hypercorrosion in the gold plating bath.<sup>13</sup> The presence of “black pad” on a PCB means that any resulting solder joint between a PCB and electronic component upon assembly is susceptible to brittle fracture. As the immersion coating of Au is dependent on the efficient removal of Ni from the surface, these plating solutions are typically run at an acidic pH which means the conventional aqueous immersion gold process fundamentally contributes to the formation of these defects and control over when and where they form is difficult.<sup>14</sup> To address these issues, Deep Eutectic Solvents (DES) have shown promise in the immersion coating of other metals, such as copper, from acid free formulations<sup>15-17</sup> and so our strategy has been focused on the development of alternative processes using DES media.

DESs are a novel class of solvents similar to ionic liquids (ILs). Whereas ILs are composed exclusively of ions, DESs are liquids composed of a salt and complexing agent, commonly a tetraalkylammonium salt, such as choline chloride, and a hydrogen bond donor (HBD), such as 1,2-ethanediol or urea. When mixed together the HBD binds to the anion resulting in a large depression of the melting point.<sup>18</sup> These liquids have widespread appeal in the electrochemical, synthetic and polymer fields due to their low toxicity, they are air and moisture stable and are easily prepared in high purity.<sup>15</sup> We have previously demonstrated a variety of electrolytic coatings including Ni,<sup>19</sup> Cu, Cr, Ag, Sn and Zn at high current efficiency.<sup>20</sup> In addition, an immersion Ag deposition onto copper<sup>10</sup> as an alternative PCB surface finish was studied, including scale up to pilot plant scale, demonstrating its suitability for the industrial production of PCBs.<sup>17</sup>

Ionic liquids have been used to study the electrochemical dissolution/deposition of gold as a method for avoiding the use of cyanide.<sup>21-23</sup> In addition Qin et al. have studied the immersion deposition of gold from tetrachloridoauric acid in the ionic liquid butylmethylimidazolium hexafluorophosphate onto zinc substrate.<sup>24</sup> Wang et al. showed that uniform and bright ENIG coatings could be obtained from a solution of 500 g L<sup>-1</sup> choline chloride in water adjusted to pH 2 with HCl and 1 g L<sup>-1</sup> tetrachloridoauric acid.<sup>25</sup> However, the low pH of this system means that the mechanism by which “black pad” occurs is still present and may still be a problem if used in PCB production.

Metal speciation is important, as the solution phase structure of a dissolved metal salt can affect its electrochemical properties and solubility, hence altering the plating characteristics.<sup>2</sup> Extended X-ray absorption fine structure (EXAFS) spectroscopy has been used to elucidate and study the speciation of metal salts in IL and DES environments, where the metal salt is either an integral component of the liquid, such as the chloridometallate<sup>26-29</sup> ILs or urea:CrCl<sub>3</sub>·6H<sub>2</sub>O eutectic mixtures,<sup>30</sup> or where the metal salt is a solute dissolved in eutectic mixtures, such as Ethaline 200 (a 2:1 molar ratio of 1,2-ethanediol:choline chloride).<sup>31-34</sup> For example, we have previously studied the speciation of a wide range of metal chloride salts in the DES mixtures formed from a 1:2 molar ratio of choline chloride with either 1,2-ethanediol, 1,2-propanediol or 1,3-propanediol.<sup>33</sup> In the majority of cases, the speciation of the metal salt is dominated by the high concentration of chloride ion in the DES, producing relatively low coordination number complexes in solution. For example, a 0.1 M solution of CuCl<sub>2</sub>·2H<sub>2</sub>O in a 1:2 choline chloride:1,2-ethanediol mixture forms tetrahedral [CuCl<sub>4</sub>]<sup>2-</sup> anionic species. Interestingly, similar effects can be observed in aqueous media through the addition of a high concentration of NaCl/LiCl/ChCl/HCl, although in most cases some water ligands remain in the first coordination shell.<sup>32, 35</sup> In some DES systems we have, however, observed that alternative speciation is possible, despite the presence of ca. 4.25 M Cl<sup>-</sup>. For example, when NiCl<sub>2</sub>·6H<sub>2</sub>O is dissolved in the DES Ethaline 200, a cationic species is formed with three neutral 1,2-ethanediol ligands directly coordinated to the nickel [Ni(HOCH<sub>2</sub>CH<sub>2</sub>OH)<sub>3</sub>]<sup>2+</sup>.<sup>33</sup> In addition, liquids formed from mixtures of CrCl<sub>3</sub>·6H<sub>2</sub>O and urea were also reported to form a cationic chromium complex.<sup>30</sup>

In this context we have been keen to understand the role of metal (Au) ion speciation in DES in the forming of galvanic deposits. In particular we have sought to correlate the electrochemical properties of different metal ion salts with a knowledge of coordination environment derived from EXAFS measurements. Further, we aim to understand the influence of metal ion speciation on the process of galvanic deposition, with the strategic goal of identifying a cyanide-free galvanic deposition of gold in DES.

In this study we compare the electrochemical properties of the gold salts AuCl, AuCN and KAu(CN)<sub>2</sub> in the DES Ethaline 200. EXAFS methods were used to characterise the solution phase coordination of the respective salts, indicating the extent to which ligand exchange of CN<sup>-</sup> for Cl<sup>-</sup> occurs in these liquids. This combined electrochemical and structural study provides insights into variations in the bulk immersion gold coatings onto electroless nickel substrates.

## Experimental

Ethaline 200 was made in an analogous method to that reported previously<sup>19</sup> using 139.63 g (1 mol) choline chloride (Aldrich) with 124.14 g (2 mol) 1,2-ethanediol (Aldrich). 5 mM DES solutions were prepared by dissolving 11.6 mg AuCl

(Aldrich), 11.1 mg AuCN (Alfa Aesar) or 14.4 mg KAu(CN)<sub>2</sub> (Alfa Aesar) in 10 ml Ethaline 200.

Cyclic voltammetry was carried out using a 2 mm diameter Pt disc working electrode, Pt flag counter electrode and a silver wire reference electrode, acting as a pseudo Ag<sup>+</sup>/Ag reference due to the high concentration of Cl<sup>-</sup> ions in the liquid. All solutions were maintained at constant temperature during electrochemical measurements *via* the use of a thermostatically controlled aluminium heating block.

In order to have a suitable surface for Au deposition, both the quartz crystal microbalance (QCM) quartz crystals (International Crystal Manufacturing Co., Oklahoma City) and copper hull cell test panels (Schloetter) were first coated in copper, followed by a layer of electroless nickel (EN), using the following method; the Cu Hull cell test panels were first cut into 2 x 6 cm strips. All samples were prepared for copper electrodeposition by immersing in Anapol Cleaner C, followed by immersion in a 0.87 M (NH<sub>4</sub>)<sub>2</sub>S<sub>2</sub>O<sub>7</sub> (Aldrich) and 0.2 M H<sub>2</sub>SO<sub>4</sub> (Fisher) solution for 1 min. Between each stage the substrate was washed thoroughly with deionised water. Copper electrodeposition was carried out at a rate of 2 A dm<sup>-2</sup> for 12 mins at room temperature in a solution of 0.57 M CuSO<sub>4</sub>·6H<sub>2</sub>O (Aldrich), 1 M H<sub>2</sub>SO<sub>4</sub> (Fisher) and 1 M ethanol (Fisher), with an iridium oxide-coated titanium mesh counter electrode.

The Cu-coated samples were prepared for EN plating by immersion in a persulfate solution identical to that detailed above, followed by a 0.5 mM PdCl<sub>2</sub> (Aldrich) solution with 0.05 M H<sub>2</sub>SO<sub>4</sub> (Fisher), and finally a 1 M H<sub>2</sub>SO<sub>4</sub> solution. The electroplated copper sample was placed into these aqueous solutions for 1 minute each and washed thoroughly after each step with deionised water. After the Cu-coated samples had been activated for EN deposition, they were transferred to a bath containing 0.1 M NiSO<sub>4</sub> (Aldrich), 0.25 M NaPH<sub>2</sub>O<sub>2</sub> (Aldrich), 0.4 M glycine (Aldrich) and 0.1 M malonic acid (Aldrich), for 45 mins at 80 °C. The EN bath was adjusted to pH 4.5 using concentrated KOH solution.

Au coatings were deposited from their respective solutions by immersing the Ni-coated sample in the solution at 80 °C for 45 mins.

Acoustic impedance QCM experiments were carried out using gold film electrodes that had been evaporated onto polished 10 MHz AT-cut quartz crystals (International Crystal Manufacturing Co., Oklahoma City). The crystals were then glued using silicon glue to the end of a glass tube of diameter 14.5 mm. The piezoelectric active electrode area was 0.23 cm<sup>2</sup>. The Au electrode in contact with the solution phase was electroplated with copper and EN as per the experimental described above. Crystal impedance spectra were recorded using a Hewlett Packard HP8751A network analyser, connected to a HP87512A transmission/reflection unit via a 50 Ω coaxial cable, such that the centre of the spectrum was near the resonance. The sweep width was 150 kHz. Experimental data were recorded as to directly replicate the plating procedures on standard Cu pieces. Solution temperature was 80 °C with measurements being taken over a 45 min timescale. Experiments were performed as soon as possible (ca. 5 mins) after Ni plating had finished to minimise oxidation. Measured data were fitted to a Lorentzian equivalent circuit model, as reported previously.<sup>37</sup>

The Au-speciation of 100 mM samples of AuCl, AuCN and KAu(CN)<sub>2</sub> was determined by extended X-ray absorption fine structure (EXAFS); B18 (Diamond synchrotron) was used for the AuCl-samples and SpLine beamline (BM25A) of the ESRF synchrotron was used for all other samples. 100 mM solutions were used to provide a suitable signal/noise ratio as opposed to 5 mM solutions as used in the electrochemical and bulk deposition studies. Measurements were carried out at the Au L<sub>III</sub>-edge, nominally 11919 eV. Transmission data were measured using ionisation chamber detectors, whilst fluorescence data were measured with a 13 element Ge solid state detector (Diamond) and a 13 element silicon SGX Sortectech detector (ESRF). A double crystal Si(111) monochromator was used. Solid reference samples for amplitude calibration were made of AuCN and AuCl in cellulose and BN matrix, respectively. The liquid samples were kept in a static flat Perspex sample holder with a sample chamber of 15 × 8 mm, at 1.5 mm thick, with 40 μm Kapton foil windows. The samples were aligned at approximately 55° with respect to the X-ray beam, with the fluorescence detector positioned perpendicular to the beam to minimise any elastic scattering signals. Two to four spectra were recorded for every sample, then averaged, calibrated and background subtracted with the program Athena.<sup>36</sup> The EXAFS spectra were fitted with Artemis to calculate interatomic distances and their root mean square deviation (σ<sub>2</sub>). Electron scattering parameters were calculated to determine type and number of coordinating atoms. Quoted uncertainties on fitted parameters are equal to two standard deviations.

Scanning electron microscope (SEM) images were recorded with a Phillips XL-30 Field Emission Gun SEM equipped with a Bruker AXS XFlash 4010 EDS detector operating at 25 kV. Secondary electron imaging (SEI) was performed with a working distance of ca. 5 mm and accelerating voltage of ca. 20 kV. Atomic force microscopy (AFM) images were acquired using a Digital Instruments (DI) Nanoscope IV, Dimension 3100 instrument using resonant (tapping) mode (software version 6.12). Surface area difference was calculated using the Nanoscope software. Sample cross sections were prepared by depositing a layer of electrolytic Ni from Watts nickel solution<sup>37</sup> at 2 V for 40 mins onto the Au-coated sample to prevent smearing of the gold deposit during polishing. This sample was then cut in a guillotine to 20 x 10 mm and encased in conductomount (MetPrep) on a Stuers Labopress-3 with heating at 180 °C for 3 mins and a force of 25 kN, followed by water cooling for 3 mins. Afterwards, the cylindrical sample was ground on 240 grit silicon carbide abrasive discs until the plated copper sheet was reached. This was then polished with increasing grit SiC discs, followed by a series of abrasive diamond suspensions reducing in size from 6 μm to 1 μm (MetPrep) with a final polishing step using 0.05 μm alumina.

## Results and Discussion

### Electrochemical behaviour

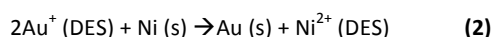
In aqueous systems gold(I) chloride will spontaneously disproportionate to gold metal and AuCl<sub>3</sub><sup>1</sup> as in the following reaction: 3Au<sup>+</sup> → Au<sup>3+</sup> + 2Au (s), unless a salt formed from a strong ligand, such as the dicyanidoaurate anion, is used. However, we have demonstrated previously that low oxidation state metal ions

are stabilised in DESs due to their high chloride activity. For example both copper(I) chloride and gold(I) chloride form stable complexes when dissolved in the DES Ethaline 200, a 1:2 molar mixture of choline chloride and ethylene glycol, under atmospheric conditions.<sup>38</sup>

Cyclic voltammetry (CV) can provide information regarding the thermodynamic, kinetic and diffusion properties of a system. These can directly affect the behaviour of the various electrochemical plating methods detailed above and measuring the CVs of AuCl, AuCN and KAu(CN)<sub>2</sub> in Ethaline 200 provides an insight into the impact of altering the cyanide content of the respective Au(I) salts.

**Figure 1** shows the cyclic voltammogram at 25 °C for 5 mM solutions of AuCl, AuCN and KAu(CN)<sub>2</sub> at a Pt disc electrode referenced to Ag wire. AuCl shows a typical, chemically reversible, deposition/stripping response that is limited by diffusion after an extended time period [The term “chemically reversible” refers to the equimolar deposition and stripping of metal at the electrode surface during the cathodic and anodic (respectively) sweeps of the voltammogram *i.e.* the metal that is deposited during reduction is removed to an equivalent extent during oxidation. This is used so as not to imply electrochemical/thermodynamic (Nernstian) reversibility]. Both AuCN and KAu(CN)<sub>2</sub> have markedly different responses. The AuCN shows no discernible Au deposition peak, suggesting that the inclusion of cyanide into the Au salt has altered the deposition characteristics so that they are kinetically controlled. Some deposition still takes place, as the reverse scan shows a peak for the oxidation of deposited Au metal. The peak area of this stripping is equivalent to a charge of 10.1 mC, compared with that of 99.0 mC for AuCl, indicating that much less Au has been removed and hence much less Au was deposited on the initial negative sweep. This is despite the AuCN voltammogram being swept to a more cathodic potential of -0.7 V compared to +0.05 V for AuCl. The difference between KAu(CN)<sub>2</sub> and AuCl in Ethaline 200 is even more pronounced with no discernible deposition/stripping peaks seen, showing that very little Au was deposited over the timescale of the experiment. This is similar to that reported for KAu(CN)<sub>2</sub> in aqueous media, where again few discernible deposition/stripping peaks are seen in the cyclic voltammograms.<sup>39</sup>

**Figure 1** also shows the cyclic voltammogram of a 5 mM nickel chloride solution in Ethaline 200. No distinct deposition/stripping behaviour can be seen over the available potential window of the solvent. The potential limits of the solvent are reached upon scanning more cathodic than -0.8 V, or more anodic than +1.25 V whereupon large currents are observed corresponding the electrolysis of the DES. In aqueous systems the  $E_0$  value for the Ni<sup>2+/0</sup> couple w.r.t. AgCl/Ag is -0.47 V<sup>9</sup>, thus, the deposition / dissolution behaviour of Ni in Ethaline 200 is kinetically controlled rather than diffusion controlled.



The relative kinetics of deposition / dissolution are of key importance for the deposition behaviour of immersion coatings, where galvanic exchange is driven by exchange of electrons from a metal substrate to a salt of a more noble metal in solution, **Equation 2**. In such galvanic processes the rate of metal dissolution and metal plating are balanced by electron stoichiometry but the

mechanistics are influenced by the speciation of the metal ion such that deposition can occur either where the depositing metal prefers to deposit on itself (gold on gold in this case) rather than on the underlying the substrate (Nickel here). Alternatively the depositing metal may prefer the substrate if the nucleation kinetics are favourable. In each of these two scenarios the morphology of the deposit may be substantially different, varying in homogeneity of deposition, adhesion of coating and morphology.

In this respect we have studied the effect of gold salt speciation on immersion coating of gold onto an EN substrate, an important process in the metal plating industry.<sup>40</sup>

### Speciation

It was observed in cyclic voltammetry experiments that, as the proportion of cyanide ligands in a gold salt increased, their electrochemical behaviour in Ethaline 200 altered significantly. The speciation of metal complexes is known to have a strong influence on their electrochemical behaviour, solubility and redox potentials.<sup>41</sup> Therefore, EXAFS measurements were carried out to determine the speciation of AuCl, AuCN and KAu(CN)<sub>2</sub> in Ethaline 200, and identify how much CN<sup>-</sup> was coordinated to the gold and to what extent ligand exchange had taken place. EXAFS has the advantage of being able to probe *in situ* the local coordination environment around a metal centre in a liquid sample, without destruction of the sample. The parameters obtained from the data fits are displayed in **Table 1**, and the proposed species are displayed in **Figure 2**.

The Fourier transform (FT) of the EXAFS data, **Figure 3 (a)**, for the AuCl solution displayed a single peak, which was fitted with a coordination of 2.0(1) chloride ligands with a Au–Cl bond length of 2.267(6) Å.<sup>33</sup> Earlier studies showed that the other group 11 metals in Ethaline 200 formed a mixture of [MCl<sub>2</sub>]<sup>-</sup> and [MCl<sub>3</sub>]<sup>2-</sup>. This behaviour is similar to that observed in aqueous brines.<sup>35, 42</sup> The observed electrochemical behaviour for AuCl in Ethaline 200 is also similar to that observed for the Ag<sup>+/0</sup> and Cu<sup>+/0</sup> redox couples, with well-defined, chemically reversible deposition and stripping behaviour.<sup>38, 43, 44</sup>

Multiple peaks are visible in the FT for the KAu(CN)<sub>2</sub> solution, **Figure 3 (c)**, suggesting coordination with two cyanide ligands. This speciation is also observed for KAu(CN)<sub>2</sub> in both aqueous and quaternary ammonium salt solutions.<sup>39</sup> EXAFS data were fitted with a multiple scattering model containing a linear dicyanide complex, which is common for the singly charged group 11 metal ions.<sup>35, 42</sup> This indicates that, despite the high concentration of chloride in the DES and unlike copper-thiocyanate,<sup>33</sup> no ligand exchange is taking place. The lack of reduction or oxidation peaks in the voltammetry, in contrast with that of the AuCl solution, suggests that the speciation of the dissolved cyanide complex in Ethaline 200 is different from that of AuCl and this is confirmed by the EXAFS data.

AuCN is sparingly soluble in aqueous media unless additional complexation agents are present, such as CN<sup>-</sup> or a halide.<sup>45</sup> In contrast, AuCN was readily soluble in Ethaline 200 due to the presence of coordinating species as a component of the bulk liquid. Accordingly, the FT of the AuCN solution data, **Figure 3 (b)**, displays three distinct peaks, which could be fitted to a mixed coordination of both Cl<sup>-</sup> and CN<sup>-</sup>, in a 1:1 ratio. This is consistent with the

electrochemistry of AuCN in Ethaline 200, where intermediate behaviour between that of the pure chloride-complex  $[\text{AuCl}_2]^-$ , and that of the pure cyanide-complex  $[\text{Au}(\text{CN})_2]^-$  is observed.

The Au-Cl bond lengths are consistent between the pure chloride complex and the mixed chloride/cyanide complex. In contrast, the Au-C bonds are longer in the dicyanide complex, but are still comparable to the solid crystal structure.<sup>46</sup> This is expected for cyanide ligands in the trans position, as the Au-C bonds will become weakened. The variations in bond length indicate that gold in the AuCN sample is actually coordinated by both chloride and cyanide and is not simply a mixture of pure cyanide and pure chloride complexes.

The electrochemical behaviour correlates directly with the evolution of the dissolved gold speciation. With greater levels of cyanide in the dissolved gold species, the relative kinetics are slower, manifesting as a change in the cyclic voltammogram from a diffusion limited response for  $[\text{AuCl}_2]^-$ , to a kinetically limited deposition for  $[\text{AuCl}(\text{CN})]^-$ , to no discernible deposition/stripping at all for  $[\text{Au}(\text{CN})_2]^-$ .

### Quartz Crystal Microbalance Studies

Variations in gold deposition rates were studied using quartz crystal microbalance acoustic impedance methods. The quartz crystal microbalance (QCM) is a method where mass change on a metal surface can be measured *in situ* with nanogram resolution. QCM enables the study of mass deposited onto a quartz crystal surface by comparing the resonating frequency on the application of an AC potential across the crystal surface. An increase in mass on the crystal reduces the resonating frequency. This change is approximately linear for small mass changes of  $<5\% f_0$ , as demonstrated by the Sauerbrey equation shown in **Equation 3**, where  $\Delta f$  is the change in frequency (/Hz),  $\Delta m$  is the change in mass (g),  $f_0$  is the fundamental frequency of the crystal (/Hz),  $A$  is the piezoelectrically active surface area ( $\text{cm}^2$ ),  $\rho_q$  is the density of quartz ( $\text{g cm}^{-3}$ ) and  $\mu_q$  is the shear modulus of the quartz crystal ( $\text{g cm}^{-1} \text{s}^{-2}$ ). For a 10 MHz AT-cut quartz crystal the Sauerbrey equation simplifies to give  $\Delta f = -1.1\Delta m$  where the mass is in ng.<sup>47</sup>

$$\Delta f = \frac{-2\Delta m f_0^2}{A\sqrt{\rho_q \mu_q}} = -1.1\Delta m \quad (3)$$

Gold coated AT cut quartz crystals were used for these experiments. In order to prepare the crystal with the required nickel surface for subsequent immersion gold coating, a layer of electrolytic copper, followed by a layer of EN, was coated onto the crystal as per the methodology detailed in the experimental. The commercial protocol for EN deposition (described in the experimental section) was used in order to maintain consistency with any potential PCB applications. In a typical copper electrodeposition experiment the mass of copper deposited was 1.4 mg, which corresponds to a thickness of 7.97  $\mu\text{m}$ . In the subsequent EN deposition the mass of Ni deposited was 0.2 mg, which corresponds to a thickness of 1.1  $\mu\text{m}$ . For each of these calculations measurements were made from the dry crystal.

The electroless Ni deposited onto the Cu coated crystal was used as a standard coating from which to compare the relative deposition rates of Au from various Au salts in Ethaline 200. In a typical

experiment the dry crystal resonance was recorded and monitored at 8.5 s intervals. The crystal was then transferred to the Au plating solution for 45 mins to allow immersion Au coating to take place. **Figure 4 (a)** shows the fitted acoustic impedance resonance response for the 1<sup>st</sup> scan after immersion into a 5 mM AuCl solution in Ethaline 200 and the subsequent responses at 40 scan intervals. The peak frequency decreases as the experiment progresses, corresponding to an increase in mass on the crystal surface due to the immersion deposition of Au.

**Figure 4 (b)** shows the mass increase on the crystal surface with time for solutions of Ethaline 200 containing the three gold salts as detailed in **Table 2**. Each of the solutions appear to have a linear response of deposition rate with time with deposition rates of 1.16, 0.76 and 0.37  $\text{nm min}^{-1}$  for the AuCl, AuCN and  $\text{KAu}(\text{CN})_2$  solutions respectively. It is worth noting that the initial rate of AuCl deposition is much faster than 1.16  $\text{nm min}^{-1}$  but after 100 s the rate is independent of time. During this experiment the solution became turbid and analysis of the coating after the experiment showed poor adherence, so the rate shown by QCM measurements may be lower than the true rate due to Au particles detaching from the surface during measurement. The deposition rate from the AuCN solution was 0.76  $\text{nm min}^{-1}$  and the deposition rate from the  $\text{KAu}(\text{CN})_2$  solution was 0.37  $\text{nm min}^{-1}$ . This trend follows the deposition behaviour of the gold from these salts in Ethaline 200 when studied electrochemically, showing a significant reduction in the plating rate as the dissolved anionic gold species contains progressively more cyanide.

### Bulk Coating

Having observed the impact of speciation on Au electrochemistry and rate of deposition in immersion coatings onto EN, we then investigated how Au speciation affects coating morphology **Figure 5**. Identical conditions to the QCM study were employed.

The fabrication process for the samples is shown in **Scheme 1**. After EN deposition the samples were used in subsequent immersion Au plating immediately to minimise oxidation of the Ni. 5 mM AuCl in Ethaline 200 was used to produce sample **1**, 5 mM AuCN to produce sample **2** and 5 mM  $\text{KAu}(\text{CN})_2$  to produce sample **3**. In each case the immersion Au experiments were run for 40 mins at 80 °C for consistency.

**Figure 5** shows a photo of samples **1**, **2** and **3**. Sample **1** shows a very rough deposit which was also poorly adherent. The gold coating was easily removed using adhesive tape (Sellotape) revealing the electroless Ni substrate surface. Sample **2** produces a gold coloured sample similar but slightly brighter and more yellow than **1**, showing a thick, uniform and adherent coating across the EN surface. Sample **3** shows a uniform Au coating, although it is notably greyer and duller in character showing the gold layer is thin and / or not in total surface coverage of the EN surface.

SEM analysis, shown in **Figure 6**, provides greater detail with regards to the structure of the immersion Au coatings in these samples. **Figure 6 (a)** show the underlying amorphous, nodular structure of the EN substrate. EDX analysis shows the presence of 87 wt% Ni and 12.9 wt% P which stoichiometrically equates to approximately  $\text{Ni}_4\text{P}$  (the phosphorus content is incorporated from the reducing agent and is consistent with expectation for this

coating). Importantly, the uniform surface shows that any additional features observed after gold plating are due to the immersion gold coating altering the structure and morphology of the surface. The SEM image in **Figure 6 (b)**, from sample **1**, shows the presence of some small particles on the surface of the EN nodules. However, **2** shows only small surface features related to the Au deposition and sample **3** shows no discernible features, aside from the nodular nickel substrate structure.

In order to better quantify the structure variations between the samples, and obtain values for surface roughness, atomic force microscopy (AFM) was used to obtain height profiles of the three gold coatings, as shown in **Figure 7**. **Figure 7 (a)** shows the AFM image of a  $20\ \mu\text{m}^2$  area of electroless nickel substrate where a similar smooth, nodular nickel is observed. This is consistent with the SEM images, **Figure 6**, and is characteristic of all of these samples. This work is specifically interested in the surface features attributed to the Au coating rather than the EN layer and the SEM analysis from **Figure 6** shows that surface features from the Au are much smaller than the EN nodules of the substrate. Therefore, images recorded over a much smaller surface area provide more detail regarding the fine structure of the Au surface.

**Figure 7 (b)** shows the same EN coating at a surface area of  $2\ \mu\text{m}^2$ . Very few features aside from the EN nodules are apparent. **Figure 7 (c)**, the coating from **1**, shows a marked increase in the roughness of the surface due to the Au layer that has been deposited on the EN, in which some micron scale crystallites are visible in the image. Standard methods for measuring surface roughness include using the values  $R_a$  or  $R_q$ .<sup>48</sup> Both of these measurements are based on the deviation of the sample from the mean height. In this case the biggest contributor to the values of  $R_a$  and  $R_q$  are the electroless Ni nodules which have a variation in height of up to  $1\ \mu\text{m}$ . QCM analysis shows that expected Au coating thicknesses are below  $100\ \text{nm}$  but the  $R_a$  and  $R_q$  values for **Figure 7 (a)** are  $224\ \text{nm}$  and  $270\ \text{nm}$  respectively. Because of this the % surface area difference (%SAD) has been used for comparison of the roughness. The %SAD is measured by dividing the measured topographical surface area,  $A_m$ , determined by the AFM, by the geometric footprint over which it was recorded,  $A_g$ . This is defined in **Equation 4**.

$$\%SAD = \left( \frac{A_m}{A_g} - 1 \right) \times 100\% \quad (4)$$

The %SAD for the EN substrate across a  $2\ \mu\text{m}^2$  profile was 9.27%, this can then be used as a value by which to compare the immersion gold samples from Ethaline 200. **Figure 7 (c)** shows the image for **1**, plating from AuCl in Ethaline 200, and in this case the z axis is between  $-850$  to  $850\ \text{nm}$  due to the much larger size of the surface features. The rest of the  $2\ \mu\text{m}^2$  images have a z-axis from  $-150$  to  $150\ \text{nm}$  and thus are directly visually comparable.

SEM analysis shows the Au deposits from Ethaline 200 get progressively smaller in feature size from sample **1** to sample **3** and the AFM images also confirm this. There is a clear reduction in the height variation of the Au deposit, showing the impact that the speciation of Au has on the Au deposits. **1** has a %SAD of 180% which is substantially larger than that of **2** and **3**, which are 4.0 and

3.78% respectively. Changing the speciation of the Au salt with **1** or **2** equivalents of  $\text{CN}^-$  has the effect of dramatically reducing the roughness of the resulting Au coating as consistent with the observation seen from the SEM images.

Having carried out a comprehensive study of the surface structure of these coatings, investigations were made into the structure throughout the Au coating by examination of the cross-section. To facilitate this the samples were over-plated with a layer of Ni from a commercial Watts Ni electrolyte at a current density of  $2\ \text{A dm}^{-2}$  to prevent smearing at the edge of the respective ENIG interfaces. In our hands this methodology is successful in preserving fine structure at surfaces and interfaces where dendritic, soft or friable deposits are sufficiently robust to withstand immersion in an aqueous electrolyte *i.e* do not fall off in transit. The samples were then encased within a conducting thermosetting resin that was suitable for SEM analysis and subjected to a series of polishing steps with a final polishing with  $50\ \text{nm}$  alumina suspension to ensure that surface features were minimised.

**Figure 8** shows the respective SEM images of the cross sections from samples **1**, **2**, and **3**. The various metallic coatings for **1** have been labelled in **Figure 8 (a)** where from bottom left to top right the base Cu layer, amorphous electroless Ni, thin immersion Au and electrolytic over-plated Ni layers can be seen. The electroless Ni layer is the thickest coating in the image, with a thickness of approximately  $9\ \mu\text{m}$ . Above the Ni is a bright band which corresponds to the immersion Au deposit. Interestingly, considerable detail relating to this structure can be seen due to the electrolytic layer of Ni on the surface locking this structure into position. **Figure 8 (b)** shows a higher resolution image of this area. It is possible to see that the Au has grown in three dimensions (as opposed to the 2 planar dimensions) resulting in a dendrite-like structure. This three dimensional growth explains the large, rough and particulate nature of the coatings from AuCl in Ethaline 200. A dark band can be seen at the edge of the Ni/P and Au boundary. This is likely to be due to phosphorous enrichment of this layer during the immersion Au process. As the immersion Au process corrodes the Ni surface, resulting in the oxidation of Ni, a phosphorous enriched layer remains.<sup>49</sup> QCM studies showed that the rate of Au deposition for **1** was faster than that from **2** and **3**, and the rate may be even faster than measured due to the poor adherence of Au to the Ni/P surface, indicating that phosphorous enrichment at the Ni/Au boundary should be most prominent in this case.

In contrast, **Figures 8 (c)** and **(d)** show the high resolution images for the cross section of samples **2** and **3** respectively. In both of these images the Au is present as a uniform thin film throughout the entire sample showing that immersion coatings from these formulations show good surface coverage of uniform thickness across the coating.

As increasing levels of cyanide are introduced to a gold salt dissolved in Ethaline 200 a trend of slower deposition rate and improved coating morphology/quality is observed. This has been linked to the electrochemical behaviour of the respective gold salts when compared to that of nickel. Nickel showed no clear deposition

/ oxidation peak in the CV in **Figure 1**, indicating sluggish kinetics of deposition / dissolution.

When AuCl in Ethaline 200 is used in the galvanic exchange of nickel a rough, particulate, poorly adherent deposit forms. It is postulated that, in this case, the reaction rate determining step for Au deposition is limited by the oxidation of Ni from the surface and, as such, when Au(I) is reduced readily, there is little selectivity regarding growth sites causing the dendritic type structures identified in **Figure 8 (a)** and **(b)**. The dendrite formation is consistent with that seen by Qin et al.<sup>24</sup> when studying immersion Au coating from a solution of HAuCl<sub>4</sub> on Zn sheet in the IL butylmethylimidazolium hexafluorophosphate, who explained that this growth was due to preferential deposition of Au onto Au, as opposed to Zn. There is synergy between these two mechanisms in that lack of nucleation sites on the substrate surface causes preferential deposition of Au on Au, resulting in dendritic growth.

In contrast when cyanide is present in the gold salt the reduction of the Au(I) ions in solution begins to limit the rate of galvanic exchange, reducing the overall rate, enabling more selectivity regarding the sites of Au deposition, leading to a much more uniform coating.

The substrate surface remains consistent for each of the three samples. As such the difference in the deposition properties of these three salts is highly likely to be related to the solution phase structures that were determined through EXAFS, with the incorporation of progressively larger levels of cyanide in the anionic gold species directly leading to lower rates of galvanic exchange.

## Conclusions

A study has been carried out into the electrochemical behaviour of 5 mM solutions of AuCl, AuCN and KAu(CN)<sub>2</sub> in the DES Ethaline 200, along with an investigation of the properties of immersion coatings of gold onto standardised electroless Ni surfaces. It was observed that the electrochemical behaviour of each of these gold compounds in Ethaline 200 varied greatly, with a chemically reversible diffusion limited response seen for AuCl, whereas AuCN and KAu(CN)<sub>2</sub> showed much more complicated, kinetically limited responses. This behaviour has been rationalised by the differing speciation for each of these compounds. EXAFS shows that AuCl forms the chlorido-complex [AuCl<sub>2</sub>]<sup>-</sup>, AuCN forms a mixed [AuCl(CN)]<sup>-</sup> species, whereas KAu(CN)<sub>2</sub> maintains its [Au(CN)<sub>2</sub>]<sup>-</sup> structure. The more labile Cl<sup>-</sup> enables easier reduction of Au when compared to the tightly bound cyanide species, hence leading to slower kinetics of deposition and differing electrochemical behaviour. QCM analysis of immersion Au coatings onto electroless Ni shows that switching from a pure chloride coordinated species to a pure cyanide coordinated species leads to a threefold reduction in the plating rate. We are currently engaged in further detailed mechanistic and kinetic studies of charge/ligand transfer processes associated with the reduction of metal ions in DES and it is our aim to expand on the current study in further publications.

Bulk plating samples were prepared from the Au plating solutions onto aqueous electroless Ni at 80 °C for 45 mins. The AuCN in DES solution gave a bright gold coating, the KAu(CN)<sub>2</sub> solution give a visibly thin coating, whilst the coating from AuCl in Ethaline 200 was dull and poorly adhesive. AFM, surface SEM and cross section SEM showed the dramatic extent to which the morphology of these Au coatings differ.

We have shown that metal speciation in DESs can remain distinct despite the high chloride activity and that this can have a large subsequent knock-on effect on any metal deposits obtained from these solutions. In addition, these coatings are also very promising from a technological perspective as ENIG finishes in PCB industry where the elimination of acid in gold plating formulation could potentially lead to more reliable coatings. Consequently, these results are both significant and timely.

We note here that in immersion Au coatings from each of the DES formulations the plating rate is lower that of the conventional aqueous process at the same temperature. However, the ability to stabilise a wider range of Au(I) salts (in DES compared to aqueous solution) opens the possibility to cyanide free immersion Au plating and the lack of a requirement for an acid activator should minimise unwanted substrate oxidation.

## Acknowledgements

This work was supported through the EU funded research for SME's ASPIS project (FP7-SME AG-2008-2) and the German Research Foundation (DFG grant FR 3458/2-1). In addition, we would like to thank the teams of Diamond beamline B18 and ESRF beamline 25A (SpLine) for beamtime and support.

## Notes and references

1. M. Kato and Y. Okinaka, *Gold Bulletin*, 2004, **37**, 37-44.
2. M. Schlesinger and M. Paunovic, *Modern Electroplating*, Wiley, 2011.
3. S. Dimitrijević, M. Rajčić-Vujanović and V. Trujić, *International Journal of the Electrochemical Society*, 2013, **8**, 6620-6646.
4. Y. Shacham-Diamand, T. Osaka, Y. Okinaka, A. Sugiyama and V. Dubin, *Microelectronic Engineering*, 2015, **132**, 35-45.
5. A. Ballantyne, G. Forrest, M. Goosey, A. Griguceviciene, J. Juodkazyte, R. Kellner, K. Ryder, A. Selskis, R. Tarozaitė and E. Veninga, *Circuit World*, 2012, **38**, 21-29.
6. Y. Okinaka and M. Hoshino, *Gold Bulletin*, 1998, **31**, 3-13.
7. P. Wilkinson, *Gold Bulletin*, 1986, **19**, 75-81.
8. M. J. Liew, S. Roy and K. Scott, *Green Chemistry*, 2003, **5**, 376-381.
9. A. J. Bard, R. Parsons and J. Jordan, *Standard Potentials in Aqueous Solutions*, Marcel Dekker, New York, 1985.
10. A. P. Abbott, S. Nandhra, S. Postlethwaite, E. L. Smith and K. S. Ryder, *Physical Chemistry Chemical Physics*, 2007, **9**, 3735-3743.
11. G. Milad, *Circuit World*, 2010, **36**, 10-13.
12. Y. S. Won, S. S. Park, J. Lee, J.-Y. Kim and S.-J. Lee, *Applied Surface Science*, 2010, **257**, 56-61.

13. P. Snugovsky, P. Arrowsmith and M. Romansky, *Journal of Electronic Materials*, 2001, **30**, 1262-1270.
14. K. J. Zeng, R. Stierman, D. Abbott and M. Murtuza, *JOM*, 2006, **58**, 75-79.
15. E. L. Smith, A. P. Abbott and K. S. Ryder, *Chemical Reviews*, 2014, **114**, 11060-11082.
16. E. L. Smith, *Transactions of the Institute of Metal Finishing*, 2013, **91**, 241-248.
17. E. L. Smith, A. P. Abbott, J. Griffin, R. C. Harris, C. O'Connor and K. S. Ryder, *Circuit World*, 2010, **36**, 3-9.
18. A. P. Abbott, G. Capper, D. L. Davies, R. K. Rasheed and V. Tambyrajah, *Chemical Communications*, 2003, 70-71.
19. A. P. Abbott, A. Ballantyne, R. C. Harris, J. A. Juma, K. S. Ryder and G. Forrest, *Electrochimica Acta*, 2015, **176**, 718-726.
20. A. P. Abbott, G. Frisch and K. S. Ryder, *Annual Review of Materials Research*, Vol 43, 2013, **43**, 335-358.
21. X. Yang, R. Yang, D. Shi, S. Wang, J. Chen and H. Guo, *Journal of Chemical Technology and Biotechnology*, 2015, **90**, 1102-1109.
22. Y. Wang, X. Cao, W. Wang, N. Mitsuzak and Z. Chen, *Surface & Coatings Technology*, 2015, **265**, 62-67.
23. D. Jones, J. Hartley, G. Frisch, M. Purnell and L. Darras, *Palaeontologia Electronica*, 2012, **15**.
24. Y. Qin, Y. Song, N. Sun, N. Zhao, M. Li and L. Qi, *Chemistry of Materials*, 2008, **20**, 3965-3972.
25. Y. Wang, X. Cao, W. Wang, N. Mitsuzak and Z. Chen, *Surface and Coatings Technology*, 2015, **265**, 62-67.
26. A. J. Dent, K. R. Seddon and T. Welton, *Journal of the Chemical Society-Chemical Communications*, 1990, 315-316.
27. M. Currie, J. Estager, P. Licence, S. Men, P. Nockemann, K. R. Seddon, M. Swadzba-Kwasny and C. Terrade, *Inorganic Chemistry*, 2013, **52**, 1710-1721.
28. F. Coleman, G. Feng, R. W. Murphy, P. Nockemann, K. R. Seddon and M. Swadzba-Kwasny, *Dalton Transactions*, 2013, **42**, 5025-5035.
29. D. C. Apperley, C. Hardacre, P. Licence, R. W. Murphy, N. V. Plechkova, K. R. Seddon, G. Srinivasan, M. Swadzba-Kwasny and I. J. Villar-Garcia, *Dalton Transactions*, 2010, **39**, 8679-8687.
30. A. P. Abbott, A. A. Al-Barzinjy, P. D. Abbott, G. Frisch, R. C. Harris, J. Hartley and K. S. Ryder, *Phys. Chem. Chem. Phys.*, 2014, **16**, 9047-9055.
31. C. Hardacre, in *Annual Review of Materials Research*, 2005, vol. 35, pp. 29-49.
32. P. De Vreese, N. R. Brooks, K. Van Hecke, L. Van Meervelt, E. Matthijs, K. Binnemans and R. Van Deun, *Inorganic Chemistry*, 2012, **51**, 4972-4981.
33. J. M. Hartley, C.-M. Ip, G. C. H. Forrest, K. Singh, S. J. Gurman, K. S. Ryder, A. P. Abbott and G. Frisch, *Inorganic Chemistry*, 2014, **53**, 6280-6288.
34. J. Estager, J. D. Holbrey and M. Swadzba-Kwasny, *Chem. Soc. Rev.*, 2014, **43**, 847-886.
35. C. H. Gammons, Y. M. Yu and A. E. Williams-Jones, *Geochimica Et Cosmochimica Acta*, 1997, **61**, 1971-1983.
36. B. Ravel and M. Newville, *Journal of Synchrotron Radiation*, 2005, **12**, 537-541.
37. W. C. PLC, *The Canning handbook*, W. Canning Plc., Birmingham, England, 1982.
38. A. P. Abbott, G. Frisch, S. J. Gurman, A. R. Hillman, J. Hartley, F. Holyoak and K. S. Ryder, *Chemical Communications*, 2011, **47**, 10031-10033.
39. G. Ma, W. F. Yan, T. D. Hu, J. Chen, C. H. Yan, H. C. Gao, J. G. Wu and G. X. Xu, *Phys. Chem. Chem. Phys.*, 1999, **1**, 5215-5221.
40. J. W. Yoon and S. B. Jung, *Journal of Alloys and Compounds*, 2005, **396**, 122-127.
41. L. M. Moretto and K. Kalcher, eds., *Environmental Analysis by Electrochemical Sensors and Biosensors*, Springer, New York, 2015.
42. J. L. Barriada, A. D. Tappin, E. H. Evans and E. P. Achterberg, *Trends in Analytical Chemistry*, 2007, **26**, 809-817.
43. A. P. Abbott, A. A. Al-Barzinjy, P. D. Abbott, G. Frisch, R. C. Harris, J. Hartley and K. S. Ryder, *Physical Chemistry Chemical Physics*, 2014, **16**, 9047-9055.
44. A. P. Abbott, K. El Ttaib, G. Frisch, K. J. McKenzie and K. S. Ryder, *Physical Chemistry Chemical Physics*, 2009, **11**, 4269-4277.
45. M. A. Elhinnawi, L. Peter and B. Meyer, *Journal of Raman Spectroscopy*, 1985, **16**, 272-279.
46. A. Rosenzweig and D. T. Cromer, *Acta Crystallographica*, 1959, **12**, 709-712.
47. G. Sauerbrey, *Zeitschrift für Physik*, 1959, **155**, 206-222.
48. J. R. Smith, C. Larson and S. A. Campbell, *Transactions of the Institute of Metal Finishing*, 2011, **89**, 18-27.
49. M. Zequn, M. Ahmad, M. Hu and G. Ramakrishna, *Electronic Components and Technology Conference*, 2005, **1**, 415-420

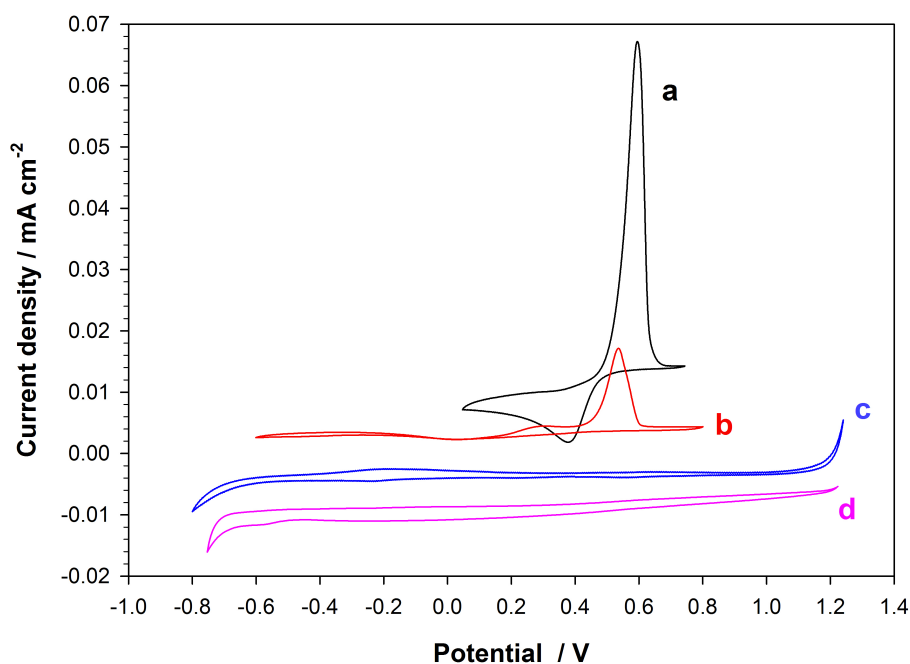


**Figure 1:** Cyclic voltammetric response of; (a) 5 mM AuCl (black), (b) AuCN (red), (c) KAu(CN)<sub>2</sub> (blue) and (d) NiCl<sub>2</sub> (pink) solutions in Ethaline 200 at a 2 mm Pt disc electrode with Pt flag counter electrode, referenced to Ag<sup>+</sup>/Ag pseudo reference, measured at room temperature with a 5 mVs<sup>-1</sup> scan rate. CVs are offset for clarity.

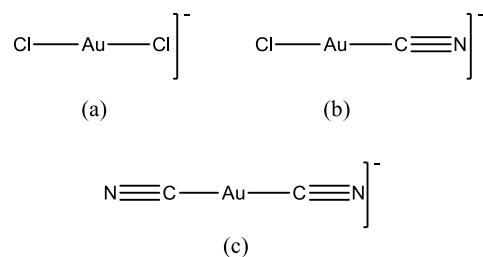


**Figure 2:** Proposed speciation of Au<sup>+</sup> in Ethaline 200 from the gold salts (a) AuCl, (b) AuCN and (c) KAu(CN)<sub>2</sub>.

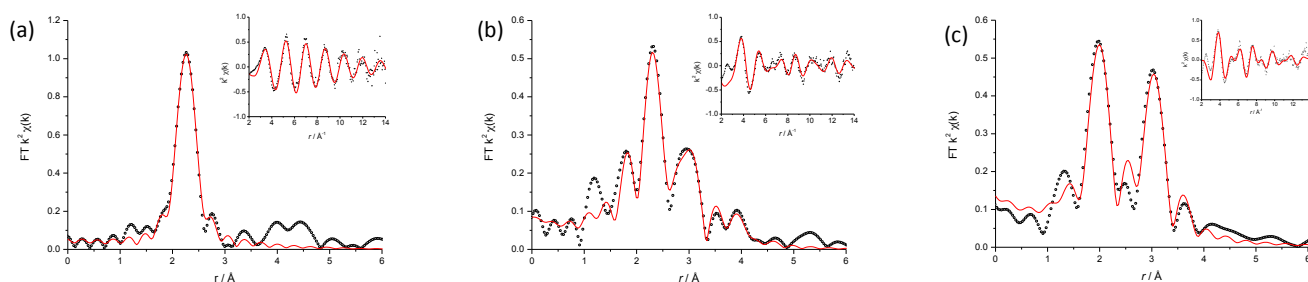


**Figure 3:** Fourier transforms of the EXAFS data (black circles) and fits for (a) AuCl, (b) AuCN and (c) KAu(CN)<sub>2</sub> in Ethaline 200. Inset: k<sup>2</sup>-weighted EXAFS spectra.

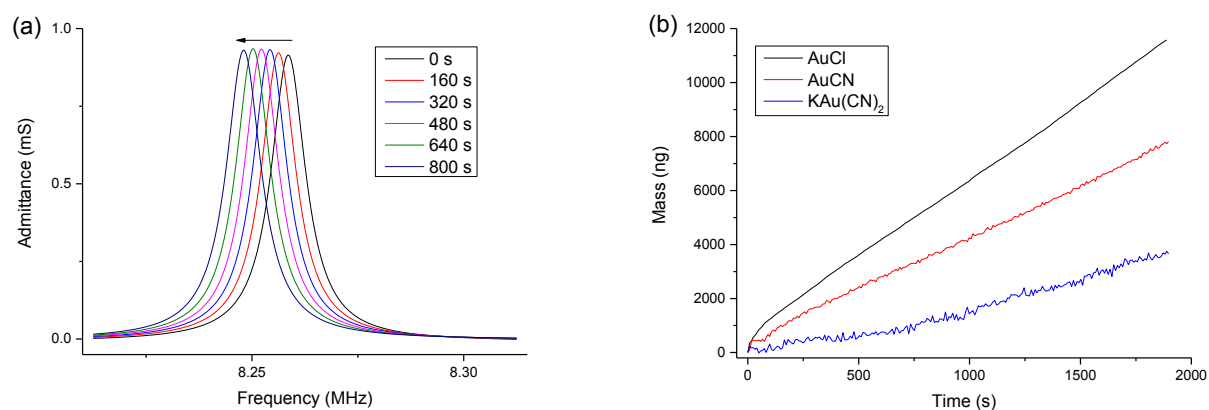


**Figure 4:** (a) Fitted frequency response of electroless Ni deposited onto a gold plated quartz crystal after 0, 160, 320, 480, 640 and 800 s when immersed in a 5 mM AuCl solution in Ethaline 200 and (b) corresponding mass changes from an electroless Ni coated quartz crystal immersed in 5 mM solutions of AuCl, AuCN and  $\text{KAu}(\text{CN})_2$  in Ethaline 200 at 80 °C.

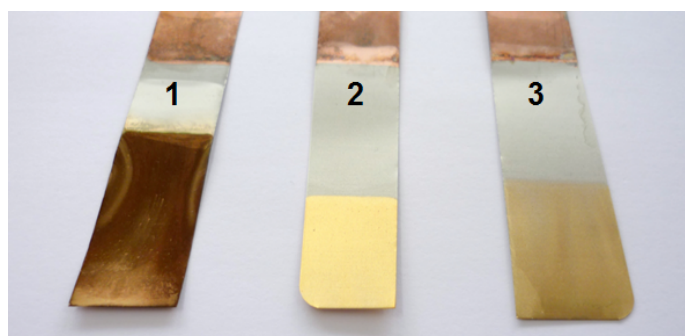


**Figure 5:** Photos of Immersion Au coatings onto electroless nickel of samples 1 (from AuCl), 2 (from AuCN) and 3 (from  $\text{KAu}(\text{CN})_2$ ).

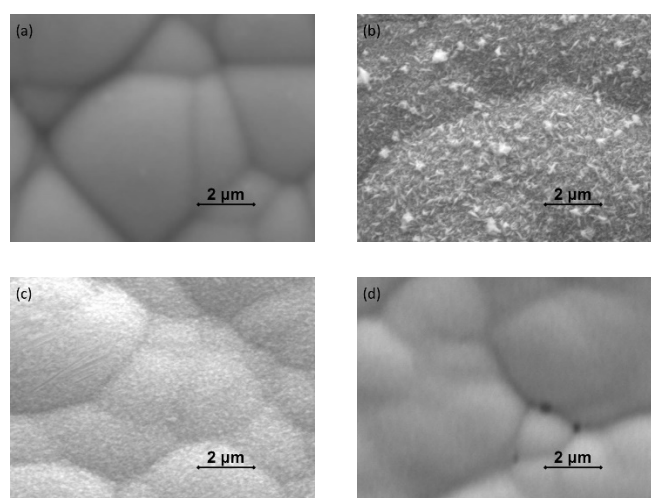


**Figure 6:** SEM images of (a) electroless nickel surface and samples (b) sample 1, (c) sample 2 and (d) sample 3 from Figure 5.

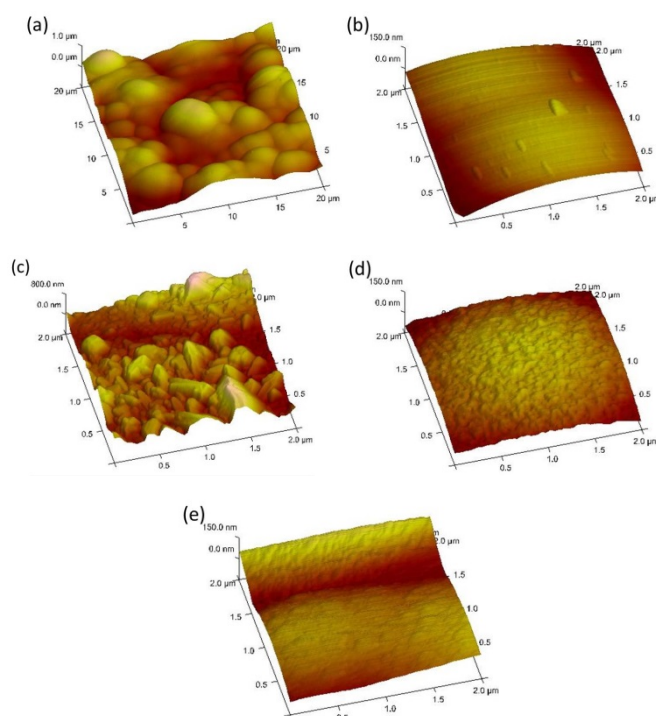


**Figure 7:** AFM images of electroless nickel substrate at (a)  $20 \mu\text{m}^2$  and (b)  $2 \mu\text{m}^2$  and the ENIG coatings at  $2 \mu\text{m}^2$  for (c) sample 1, (d) sample 2 and (e) sample 3, **Figure 5**.

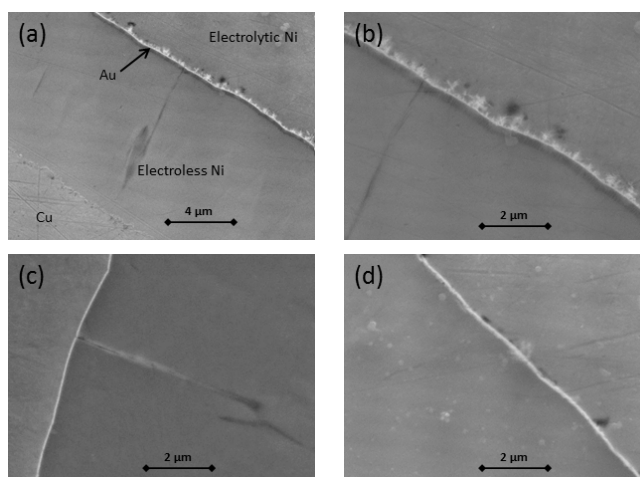
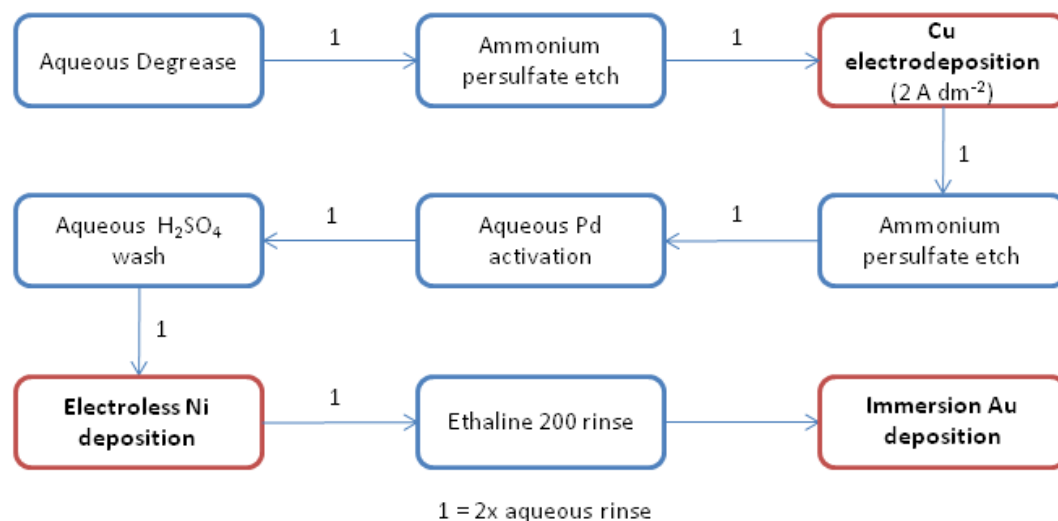


**Figure 8:** SEM cross section images of immersion Au sample for (a&b) sample 1, (c) sample 2 and (d) sample 3, **Figure 5**, where an electrolytic over-plated Ni layer was deposited onto the surface of the sample prior to sectioning.



**Scheme 1:** Fabrication process for EN samples subsequently coated in immersion gold from DES Ethaline 200.

**Table 1:** EXAFS fit parameters of 100 mM solutions of the gold salts AuCl, AuCN and KAu(CN)<sub>2</sub> in the DES Ethaline 200.

Metal salt	X	Number of atoms, N	Distance from Au, r/Å	Debye-Waller factor, $\sigma/\text{Å}^2$	Fit index, R1/%
AuCl	Cl	2.0(1)	2.267(6)	0.0031(6)	1.14 %
AuCN	Cl	1.0(2)	2.272(6)	0.003(1)	3.72 %
	C	1.1(1)	1.94(1)	0.003(2)	
	N		3.11(1)	0.005(1)	
KAu(CN) <sub>2</sub>	C	2.3(3)	1.98(1)	0.003(2)	2.43 %
	N		3.15(1)	0.003(2)	

**Table 2:** Plating rate and surface area difference measured from 2  $\mu\text{m}$  AFM images, for gold surfaces deposited from solutions of 5 mM gold salt in Ethaline 200.

Sample	Au salt	Plating Rate ( $\text{nm min}^{-1}$ )	% Surface Area Difference (2 $\mu\text{m}^2$ image)
1	AuCl	1.16	180.0
2	AuCN	0.76	4.03
3	KAu(CN) <sub>2</sub>	0.37	3.78